

# Supporting Information for ‘No consistent simulated trends in the Atlantic Meridional Overturning Circulation for the past 6,000 years’

Zhiyi Jiang<sup>1</sup>, Chris M. Brierley<sup>1</sup>, Juergen Bader<sup>2\*</sup>, Pascale Braconnot<sup>3\*</sup>, Michael Erb<sup>4\*</sup>, Peter O. Hopcroft<sup>5\*</sup>, Dabang Jiang<sup>6\*</sup>, Johann Jungclaus<sup>2\*</sup>, Vyacheslav Khon<sup>7\*,8\*</sup>, Gerrit Lohmann<sup>9\*</sup>, Olivier Marti<sup>3\*</sup>, Matthew B. Osman<sup>10\*</sup>, Bette Otto-Btiesner<sup>11\*</sup>, Birgit Schneider<sup>12\*</sup>, Xiaoxu Shi<sup>9\*</sup>, David J. R. Thornalley<sup>1\*</sup>, Zhiping Tian<sup>6\*</sup> and Qiong Zhang<sup>13\*,14\*</sup>

<sup>1</sup>Department of Geography, University College London, London, WC1E 6BT, UK

<sup>2</sup>Max-Planck-Institut für Meteorologie, Hamburg, Germany

<sup>3</sup>Laboratoire des Sciences du Climat et de l’Environnement-IPSL, Gif-sur-Yvette, France

<sup>4</sup>School of Earth and Sustainability, Northern Arizona University, Flagstaff, AZ, USA

<sup>5</sup>School of Geography, Earth and Environmental Sciences, University of Birmingham, B15 2TT, UK

<sup>6</sup>Institute of Atmospheric Physics, Chinese Academy of Sciences, Beijing, China

<sup>7</sup>Lyell Centre, Heriot-Watt University, Edinburgh, United Kingdom

<sup>8</sup>A. M. Obukhov Institute of Atmospheric Physics, Russian Academy of Sciences, Moscow, Russia

<sup>9</sup>Alfred-Wegener-Institut Helmholtz-Zentrum für Polar- und Meeresforschung, Bremerhaven, Germany

<sup>10</sup>Department of Geography, University of Cambridge, Cambridge, CB2 3EN, UK

<sup>11</sup>National Center for Atmospheric Research (NCAR), Boulder, CO, USA

<sup>12</sup>Institute of Geosciences, Kiel University, Kiel, Germany

<sup>13</sup>Department of Physical Geography, Stockholm University, Stockholm, Sweden

<sup>14</sup>Bolin Centre for Climate Research, Stockholm University, Stockholm, Sweden

\*These authors are listed in alphabetical order

## Contents of this file

1. Text S1 to S8
2. Table S1
3. Figures S1 to S2

**Introduction** The supporting text, table and figures shown here provide the supporting information for the main manuscript.

**Text S1** describes the experimental design for the transient run with AWI-ESM-2.

**Text S2** describes the experimental design for the transient run with IPSL-CM5.

**Text S3** describes the experimental design for the transient run with MPI-ESM.

**Text S4** describes the experimental design for the transient run with EC-Earth3-veg-LR.

**Text S5** describes the experimental design for the transient run with HadCM3-M2.1d.

**Text S6** describes the experimental design for the transient run with KCM.

**Text S7** describes the experimental design for the transient run with CCSM3.

**Text S8** describes the experimental design for the transient run with CESM1.2.1.

**Table S1** shows the trend and p-value (based on Student’s t-test) for (i) each simulation’s overall AMOC strength at 30°N below 500 m, (ii) each simulation’s 100-yr running standard deviation of the overall maximum AMOC strength at 30°N below 500 m with / without band-pass filter.

**Figure S1** shows the indicators of the AMOC variability for the past 2,000 years.

**Figure S2** shows the 100-yr running standard deviation of the band-pass (25-75 yr) filtered overall maximum AMOC strength at 30°N below 500 m.

**Text S1 AWI-ESM-2**

The Holocene transient simulation with AWI-ESM-2 starts from 6 ka BP to 0 ka BP (Present is defined as 1950 CE), and includes the dynamic vegetation changes in the JSBACH model. The AWI-ESM-2 model uses the ECHAM6 as the atmospheric module with a resolution of  $1.875^\circ \times 1.875^\circ$  and 47 vertical levels. The FESOM is the oceanic module in AWI-ESM-2 which has multi-resolution capability with 46 vertical levels. The oceanic resolution can be as fine as 25 km in the polar regions and along the coastlines (Shi et al., 2020). It has an orbital forcing derived from Berger (1978). The past ice core records, alongside the measurement of the atmospheric samples that conducted recently, provide the GHG concentrations for this transient run (Köhler et al., 2017). The mid-Holocene spin-up run has been integrated for 1000 model years with the AMOC in the final years being in its quasi-equilibrium state. A detailed description about this simulation can be found in Shi et al. (2020) and Sidorenko et al. (2019).

**Text S2 IPSL-CM5**

The IPSL-CM5 transient simulation covers the mid-Holocene to present (6 ka BP to 0 ka BP) with a spin-up time of 2,000 years. The IPSL-CM5 model using the LMDZ as an atmospheric component with a resolution of  $1.875^\circ \times 3.75^\circ$  and 39 vertical levels. The Oceanic component is based on the NEMO model with 31 vertical levels and a  $2^\circ \times (0.5 \sim 2)^\circ$  resolution. Finer resolutions of roughly  $0.5^\circ$  can be seen near Equator (Crosta et al., 2018). The orbital parameters are calculated from Berger (1978), with the trace gases concentrations ( $\text{CO}_2$ ,  $\text{CH}_4$  and  $\text{N}_2\text{O}$ ) stem from the ice core reconstruction data from Joos and Spahni (2008). Interactive vegetation is calculated within the model. Braconnat et al. (2019) provides a more comprehensive description of the IPSL transient simulation.

**Text S3 MPI-ESM**

The MPI-ESM model has been used to perform two Holocene transient run from 7.95 ka BP to 0.1 ka BP. The atmospheric component (ECHAM6) is run with a resolution of  $1.875^\circ \times 1.875^\circ$  (lon  $\times$  lat) and 47 vertical levels, and the ocean component MPIOM has a nominal horizontal resolution of  $1.5^\circ$  and 41 uneven vertical levels (Mauritsen et al., 2019). The interactive vegetation is obtained using the JSBACH land-surface model. The orbital parameters and GHG forcing in this run are derived from Berger (1978) and Brovkin et al. (2019) ice core records, respectively. The SLO0043 (TRSF) experiment includes solely GHG and orbital changes whereas the SLO0050 (TRAF) experiment includes additional forcings from volcanic aerosols and solar irradiance changes. The solar total and spectral irradiance are calculated based on the SATIRE model and solar-related changes in ozone are included using a simple scaling parameterisation (see Bader et al., 2020). Stratospheric sulfate aerosol injections imitating volcanic eruptions are prescribed from the Easy Volcanic Aerosol (EVA) forcing generator (Toohey et al., 2016), read annually, but calculated daily by linear interpolation. The forcing used here has been reconstructed based on ice-cores from both hemispheres to better identify volcanic eruptions with global impact on the climate (see Dallmeyer et al., 2021, for details). In addition, SLO0050 includes land-use forcing for the time period, where a reconstruction is available (i.e. 850 – 1850 CE) (Hurtt et al., 2011; Lawrence et al., 2016).

**Text S4 EC-Earth3-veg-LR**

The transient simulation with the EC-Earth3-Veg-LR model has a duration from 8 ka BP to 0 ka BP with dynamic

global vegetation (using LPJ-GUESS model (Smith et al., 2014), which is coupled to the land component). The EC-Earth3-veg-LR model using the Integrated Forecasting System (IFS) model (including a land model H-TESSEL) developed at the European Centre for Medium-Range Weather Forecasts (ECMWF) as the atmospheric component with a T159 horizontal spectral resolution (roughly  $1.125^\circ$ , approximately 125 km) with 62 vertical levels. Its ocean component is based on the Nucleus for the European Modelling of the Ocean (NEMO) model (Madec et al., 2008) which includes a sea-ice model LIM3 (Rousset et al., 2015). It has a nominal horizontal resolution of  $1^\circ$  and 75 vertical levels (Döscher et al., 2022). The orbital parameters in this run are computed using the method in Berger (1978). The greenhouse gas (GHG) concentrations are forced according to Köhler et al. (2017). More detailed information for the palaeo-simulations setup and for the description of the EC-Earth3 model are available in Zhang et al. (2021) and Döscher et al. (2022), respectively.

**Text S5 HadCM3-M2.1d**

The HadCM3-M2.1d (Valdes et al., 2017) Holocene transient run spans almost the entire Holocene period, from 10 ka BP to 0 ka BP. The HadCM3 model has an atmospheric resolution of  $3.75^\circ \times 2.5^\circ$  with 19 vertical levels, and an oceanic resolution of  $1.25^\circ \times 1.25^\circ$  with 20 vertical levels. This transient simulation considers the dynamics of the vegetation according to the TRIFFID Dynamic Global Vegetation Model (Cox, 2001). The orbital forcing is derived from Berger (1978), and the ice core records provide the GHG forcing (Louergue et al., 2008; Veres et al., 2013; Bereiter et al., 2015). The global ICE-6G\_C (VM5a) model is used for obtain the ice-sheet and sea-level forcing (Argus et al., 2014; Peltier et al., 2015). The xokm series used here includes palaeo-informed updates to atmospheric parameters (particularly convective entrainment/detrainment) and dynamic vegetation moisture stress. This model version therefore captures the greening of the Sahara. Further details of the model setup are described in Hopcroft and Valdes (2021).

**Text S6 KCM**

The Holocene transient simulation with KCM consists of the atmospheric general circulation model ECHAM5 (Roeckner et al., 2003) with a horizontal resolution of T31 ( $3.75^\circ \times 3.75^\circ$ ) and 19 vertical levels, coupled to the ocean sea-ice model NEMO/LIM2 (Madec et al., 2008) with a horizontal resolution of  $2^\circ \times 2^\circ$  with 31 vertical levels, and enhanced meridional resolution of  $0.5^\circ$  close to the Equator. The KCM model simulates reasonably well a present-day mean climate (Park et al., 2009) and its variability, as well as changes of the hydrological cycle during the Holocene as indicated by lake level data (V. Khon et al., 2010). The KCM has been used extensively for palaeomodeling studies, in particular to simulate the last interglacial climate (V. Khon et al., 2010; Schilt et al., 2010; Salau et al., 2012; Jin et al., 2014; V. C. Khon et al., 2018). This KCM Holocene transient simulation is forced by varying orbital parameters (eccentricity, obliquity and precession) following Berger and Loutre (1991). The GHG concentrations are obtained from the PMIP database based on ice cores from the EPICA site (Augustin et al., 2004). Changes in total solar irradiance (TSI), sea level, changes in ice sheets (neither topography nor albedo), freshwater input into the North Atlantic, or volcanic aerosols are not considered in this transient simulation (Segschneider et al., 2018). More thorough descriptions for the orbital and GHG forcing are shown in Segschneider et al. (2018).

**Text S7 CCSM3**

The TraCE-21ka simulation is a long transient run with

CCSM3 with a dynamic global vegetation model (DGVM), but without flux adjustment (Collins et al., 2006). The atmospheric model in CCSM3 is the Community Atmospheric Model 3 (CAM3), which has a resolution of  $3.75^\circ \times 3.75^\circ$  and 26 vertical levels. The ocean model is the NCAR implementation of the Parallel Ocean Program (POP). The oceanic model has 25 vertical levels and its longitudinal resolution is  $3.6^\circ$  and the latitudinal resolution is variable, with finer resolution near the equator ( $\sim 0.9^\circ$ ) (Liu et al., 2009). This simulation covers the past 21,000 years, from the Last Glacial Maximum (LGM) to present. This long-run transient simulation has successfully simulated many key deglacial climate evolutions and abrupt climate changes, which shows the model has a reasonable climate sensitivity (Liu et al., 2009). The TraCE-21ka transient simulation was started from a previous LGM simulation from Otto-Bliesner et al. (2006), the orbital parameters and associated insolation changes are computed following Berger (1978), the atmospheric GHG concentrations (carbon dioxide ( $\text{CO}_2$ ), methane ( $\text{CH}_4$ ), and nitrous oxide ( $\text{N}_2\text{O}$ )) are set based on the ice-core records from Joos and Spahni (2008). Additionally, the land ice-sheets and coastlines are forced according to Peltier (2004), and meltwater flux which sourced from the Northern Hemisphere ice-sheets to the North Atlantic and Gulf of Mexico, is calculated based on a rate that is consistent with the recorded sea-level rise record (Clark & Mix, 2002; Peltier, 2004).

#### Text S8 CESM1.2.1

The HT-11.5ka Holocene transient simulation performed with CESM1.2.1 spans from 11.5 ka to 0.1 ka BP without acceleration. It has an atmospheric resolution of approximately  $1.9^\circ \times 2.5^\circ$  with 26 vertical levels using NCAR Community Atmosphere Model version 4 (CAM4), and an oceanic resolution of approximately  $1^\circ$  horizontal grid with 60 vertical levels using the Parallel Ocean Program version 2 (POP2) (Tian et al., 2022). This transient run has its orbital parameters evolving with time throughout the Holocene according to Berger (1978). The main atmospheric GHG concentrations – carbon dioxide ( $\text{CO}_2$ ), methane ( $\text{CH}_4$ ), and nitrous oxide ( $\text{N}_2\text{O}$ ) are varying with time following Bereiter et al. (2015), Loulergue et al. (2008), and Schilt et al. (2010), respectively. The ice-sheet extent and topography changes are calculated based on the ICE-6G\_C reconstruction (Argus et al., 2014; Peltier et al., 2015). Tian et al. (2022) provides a more detailed description on this transient run.

## References

- Argus, D. F., Peltier, W., Drummond, R., & Moore, A. W. (2014). The Antarctica component of post-glacial rebound model ICE-6G\_C (VM5a) based on GPS positioning, exposure age dating of ice thicknesses, and relative sea level histories. *Geophysical Journal International*, 198(1), 537–563. doi: 10.1093/gji/ggu140
- Augustin, L., Barbante, C., Barnes, P. R., Barnola, J. M., Bigler, M., Castellano, E., ... others (2004). Eight glacial cycles from an Antarctic ice core. *Nature*, 429, 623–628. doi: 10.1038/nature02599
- Bader, J., Jungclaus, J., Krivova, N., Lorenz, S., Maycock, A., Raddatz, T., ... Claussen, M. (2020). Global temperature modes shed light on the Holocene temperature conundrum. *Nature Communications*, 11(1), 1–8. doi: 10.1038/s41467-020-18478-6
- Bereiter, B., Eggleston, S., Schmitt, J., Nehrbass-Ahles, C., Stocker, T. F., Fischer, H., ... Chappellaz, J. (2015). Revision of the EPICA Dome C  $\text{CO}_2$  record from 800 to 600 kyr before present. *Geophysical Research Letters*, 42(2), 542–549. doi: 10.1002/2014gl061957
- Berger, A. (1978). Long-term variations of daily insolation and quaternary climatic changes. *Journal of Atmospheric Sciences*, 35(12), 2362–2367. doi: 10.1175/1520-0469(1978)035<2362:ltvodi>2.0.co;2
- Berger, A., & Loutre, M.-F. (1991). Insolation values for the climate of the last 10 million years. *Quaternary Science Reviews*, 10(4), 297–317. doi: 10.1016/0277-3791(91)90033-q
- Braconnot, P., Zhu, D., Marti, O., & Servonnat, J. (2019). Strengths and challenges for transient mid-to late Holocene simulations with dynamical vegetation. *Climate of the Past*, 15(3), 997–1024. doi: 10.5194/cp-15-997-2019
- Brovkin, V., Lorenz, S., Raddatz, T., Ilyina, T., Stemmler, I., Toohey, M., & Claussen, M. (2019). What was the source of the atmospheric  $\text{CO}_2$  increase during the Holocene? *Biogeosciences*, 16(13), 2543–2555. doi: 10.5194/bg-16-2543-2019
- Clark, P. U., & Mix, A. C. (2002). Ice sheets and sea level of the Last Glacial Maximum. *Quaternary Science Reviews*, 21(1-3), 1–7. doi: 10.1016/S0277-3791(01)00118-4
- Collins, W. D., Bitz, C. M., Blackmon, M. L., Bonan, G. B., Bretherton, C. S., Carton, J. A., ... others (2006). The Community Climate System Model version 3 (CCSM3). *Journal of Climate*, 19(11), 2122–2143. doi: 10.1175/JCLI3761.1
- Cox, P. M. (2001). Description of the ‘TRIFFID’ dynamic global vegetation model. *Tech. Note 24*.
- Crosta, X., Crespin, J., Swingedouw, D., Marti, O., Masson-Delmotte, V., Etourneau, J., ... others (2018). Ocean as the main driver of antarctic ice sheet retreat during the Holocene. *Global and Planetary Change*, 166, 62–74. doi: 10.1016/j.gloplacha.2018.04.007
- Dallmeyer, A., Claussen, M., Lorenz, S. J., Sigl, M., Toohey, M., & Herzschuh, U. (2021). Holocene vegetation transitions and their climatic drivers in MPI-ESM1.2. *Climate of the Past*, 17(6), 2481–2513. doi: 10.5194/cp-17-2481-2021
- Dööscher, R., Acosta, M., Alessandri, A., Anthoni, P., Arsouze, T., Bergman, T., ... others (2022). The EC-Earth3 Earth system model for the Coupled Model Intercomparison Project 6. *Geoscientific Model Development*, 15(7), 2973–3020. doi: 10.5194/gmd-15-2973-2022
- Hopcroft, P. O., & Valdes, P. J. (2021). Paleoclimate-conditioning reveals a North Africa

- land-atmosphere tipping point. *Proceedings of the National Academy of Sciences of the United States of America*, 118(45), e2108783118. doi: 10.1073/pnas.2108783118
- Hurttt, G. C., Chini, L. P., Frolking, S., Betts, R., Feddema, J., Fischer, G., ... others (2011). Harmonization of land-use scenarios for the period 1500–2100: 600 years of global gridded annual land-use transitions, wood harvest, and resulting secondary lands. *Climatic Change*, 109(1), 117–161. doi: 10.1007/s10584-011-0153-2
- Jin, L., Schneider, B., Park, W., Latif, M., Khon, V., & Zhang, X. (2014). The spatial-temporal patterns of Asian summer monsoon precipitation in response to Holocene insolation change: a model-data synthesis. *Quaternary Science Reviews*, 85, 47–62. doi: 10.1016/j.quascirev.2013.11.004
- Joos, F., & Spahni, R. (2008). Rates of change in natural and anthropogenic radiative forcing over the past 20,000 years. *Proceedings of the National Academy of Sciences*, 105(5), 1425–1430. doi: 10.1073/pnas.0707386105
- Khon, V., Park, W., Latif, M., Mokhov, I., & Schneider, B. (2010). Response of the hydrological cycle to orbital and greenhouse gas forcing. *Geophysical Research Letters*, 37(19), L19705. doi: 10.1029/2010gl044377
- Khon, V. C., Schneider, B., Latif, M., Park, W., & Wengel, C. (2018). Evolution of Eastern Equatorial Pacific seasonal and interannual variability in response to orbital forcing during the Holocene and Eemian from model simulations. *Geophysical Research Letters*, 45(18), 9843–9851. doi: 10.1029/2018gl079337
- Köhler, P., Nehrbass-Ahles, C., Schmitt, J., Stocker, T. F., & Fischer, H. (2017). A 156 kyr smoothed history of the atmospheric greenhouse gases  $CO_2$ ,  $CH_4$ , and  $N_2O$  and their radiative forcing. *Earth System Science Data*, 9(1), 363–387. doi: 10.5194/essd-9-363-2017
- Lawrence, D. M., Hurttt, G. C., Arneth, A., Brovkin, V., Calvin, K. V., Jones, A. D., ... others (2016). The Land Use Model Intercomparison Project (LUMIP) contribution to CMIP6: rationale and experimental design. *Geoscientific Model Development*, 9(9), 2973–2998. doi: 10.5194/gmd-9-2973-2016
- Lippold, J., Pöppelmeier, F., Süfke, F., Gutjahr, M., Goepfert, T. J., Blaser, P., ... Jaccard, S. L. (2019). Constraining the variability of the Atlantic Meridional Overturning Circulation during the Holocene. *Geophysical Research Letters*, 46(20), 11338–11346. doi: 10.1029/2019gl084988
- Liu, Z., Otto-Bliesner, B., He, F., Brady, E., Tomas, R., Clark, P., ... others (2009). Transient simulation of last deglaciation with a new mechanism for Bølling-Allerød warming. *Science*, 325(5938), 310–314. doi: 10.1126/science.1171041
- Louergue, L., Schilt, A., Spahni, R., Masson-Delmotte, V., Blunier, T., Lemieux, B., ... Chappellaz, J. (2008). Orbital and millennial-scale features of atmospheric  $CH_4$  over the past 800,000 years. *Nature*, 453(7193), 383–386. doi: 10.1038/nature06950
- Madec, G., et al. (2008). NEMO ocean engine, version 3.0. *Note du Pôle de modélisation de l'Institut Pierre-Simon Laplace*, 27, 217. doi: 10.5281/zenodo.3248739
- Mauritsen, T., Bader, J., Becker, T., Behrens, J., Bitzner, M., Brokopf, R., ... others (2019). Developments in the MPI-M Earth System Model version 1.2 (MPI-ESM1.2) and its response to increasing  $CO_2$ . *Journal of Advances in Modeling Earth Systems*, 11(4), 998–1038. doi: 10.1029/2018MS001400
- Otto-Bliesner, B. L., Brady, E. C., Clauzet, G., Tomas, R., Levis, S., & Kothavala, Z. (2006). Last Glacial Maximum and Holocene climate in CCSM3. *Journal of Climate*, 19(11), 2526–2544. doi: 10.1175/JCLI3748.1
- Park, W., Keenlyside, N., Latif, M., Ströh, A., Redler, R., Roeckner, E., & Madec, G. (2009). Tropical pacific climate and its response to global warming in the KIEL climate model. *Journal of Climate*, 22(1), 71–92. doi: 10.1175/2008jcli2261.1
- Peltier, W. R. (2004). Global glacial isostasy and the surface of the ice-age earth: the ICE-5G (VM2) model and grace. *Annu. Rev. Earth Planet. Sci.*, 32, 111–149. doi: 10.1146/annurev.earth.32.082503.144359
- Peltier, W. R., Argus, D., & Drummond, R. (2015). Space geodesy constrains ice age terminal deglaciation: The global ICE-6G\_C (VM5a) model. *Journal of Geophysical Research: Solid Earth*, 120(1), 450–487. doi: 10.1002/2014jb011176
- Rahmstorf, S., Box, J. E., Feulner, G., Mann, M. E., Robinson, A., Rutherford, S., & Schaffernicht, E. J. (2015). Exceptional twentieth-century slowdown in atlantic ocean overturning circulation. *Nature climate change*, 5(5), 475–480. doi: 10.1038/nclimate2554
- Roeckner, E., Bäuml, G., Bonaventura, L., Brokopf, R., Esch, M., Giorgetta, M., ... others (2003). The atmospheric general circulation model ECHAM 5. PART I: Model description. *Max-Planck-Institut für Meteorologie internal report 349*, 144.
- Rousset, C., Vancoppenolle, M., Madec, G., Fichefet, T., Flavoni, S., Barthélémy, A., ... Vivier, F. (2015). The Louvain-La-Neuve sea ice model

- LIM3.6: Global and regional capabilities. *Geoscientific Model Development*, 8(10), 2991–3005. doi: 10.5194/gmd-8-2991-2015
- Salau, O., Schneider, B., Park, W., Khon, V., & Latif, M. (2012). Modeling the ENSO impact of orbitally induced mean state climate changes. *Journal of Geophysical Research: Oceans*, 117(C5). doi: 10.1029/2011jc007742
- Schilt, A., Baumgartner, M., Schwander, J., Buiron, D., Capron, E., Chappellaz, J., ... others (2010). Atmospheric nitrous oxide during the last 140,000 years. *Earth and Planetary Science Letters*, 300(1-2), 33–43. doi: 10.1016/j.epsl.2010.09.027
- Segschneider, J., Schneider, B., & Khon, V. (2018). Climate and marine biogeochemistry during the Holocene from transient model simulations. *Biogeosciences*, 15(10), 3243–3266. doi: 10.5194/bg-15-3243-2018
- Shi, X., Lohmann, G., Sidorenko, D., & Yang, H. (2020). Early-Holocene simulations using different forcings and resolutions in AWI-ESM. *The Holocene*, 30(7), 996–1015. doi: 10.1177/0959683620908634
- Sidorenko, D., Goessling, H. F., Koldunov, N., Scholz, P., Danilov, S., Barbi, D., ... others (2019). Evaluation of FESOM2.0 coupled to ECHAM6.3: preindustrial and HighResMIP simulations. *Journal of Advances in Modeling Earth Systems*, 11(11), 3794–3815. doi: 10.1029/2019MS001696
- Smith, B., Wårldin, D., Arneth, A., Hickler, T., Leadley, P., Siltberg, J., & Zaehle, S. (2014). Implications of incorporating N cycling and N limitations on primary production in an individual-based dynamic vegetation model. *Biogeosciences*, 11(7), 2027–2054. doi: 10.5194/bg-11-2027-2014
- Thornalley, D. J., Oppo, D. W., Ortega, P., Robson, J. I., Brierley, C. M., Davis, R., ... others (2018). Anomalously weak Labrador Sea convection and Atlantic overturning during the past 150 years. *Nature*, 556(7700), 227–230. doi: 0.1038/s41586-018-0007-4
- Tian, Z., Jiang, D., Zhang, R., & Su, B. (2022). Transient climate simulations of the Holocene (version 1)—experimental design and boundary conditions. *Geoscientific Model Development*, 15(11), 4469–4487. doi: 10.5194/gmd-15-4469-2022
- Toohey, M., Stevens, B., Schmidt, H., & Timmreck, C. (2016). Easy Volcanic Aerosol (EVA v1.0): an idealized forcing generator for climate simulations. *Geoscientific Model Development*, 9(11), 4049–4070. doi: 10.5194/gmd-9-4049-2016
- Valdes, P. J., Armstrong, E., Badger, M. P., Bradshaw, C. D., Bragg, F., Crucifix, M., ... others (2017). The BRIDGE HadCM3 family of climate models: HadCM3@ bristol v1.0. *Geoscientific Model Development*, 10(10), 3715–3743. doi: 10.5194/gmd-2017-16-rc1
- Valley, S. G., Lynch-Stieglitz, J., Marchitto, T. M., & Oppo, D. W. (2022). Seawater cadmium in the Florida Straits over the Holocene and implications for upper AMOC variability. *Paleoceanography and Paleoclimatology*, e2021PA004379. doi: 10.1029/2021pa004379
- Veres, D., Bazin, L., Landais, A., Toyé Mahamadou Kele, H., Lemieux-Dudon, B., Parrenin, F., ... others (2013). The Antarctic ice core chronology (AICC2012): an optimized multi-parameter and multi-site dating approach for the last 120 thousand years. *Climate of the Past*, 9(4), 1733–1748. doi: 10.5194/cp-9-1733-2013
- Zhang, Q., Berntell, E., Axelsson, J., Chen, J., Han, Z., De Nooijer, W., ... others (2021). Simulating the mid-Holocene, last interglacial and mid-Pliocene climate with EC-Earth3-LR. *Geoscientific Model Development*, 14(2), 1147–1169. doi: 10.5194/gmd-14-1147-2021

**Table S1.** Trend and p-value for (i) the decadally averaged overall mean AMOC strength at 30°N; (ii) the 100-yr running standard deviation of the maximum AMOC strength at 30°N below 500 m; (iii) the 100-yr running standard deviation of the filtered maximum AMOC strength at 30°N below 500 m. All the computed results are based on 6 ka to present. When filtering the AMOC time series, we applied a 25-yr to 75-yr band-pass filter, with an intention to look at the changes in multi-decadal variability. The p-value provided in this Table is adjusted p-value based on Student's t-test, for which we considered the autocorrelation in the AMOC time series and thus, adjusted the degree of freedom. The trend has unit of Sv/kyr. The trend value in bold means it is statistically significant ( $p < 0.05$ ).

Model	AMOC mean		AMOC $\sigma$		Multidecadal $\sigma$	
	trend (Sv/kyr)	p-value	trend (Sv/kyr)	p-value	trend (Sv/kyr)	p-value
AWI-ESM-2	<b>0.14</b> <sup>†</sup>	$9 \times 10^{-10}$	-0.003	0.83	-0.016	0.39
IPSL-CM5	<b>-0.138</b>	$3 \times 10^{-10}$	-0.018	0.23	-0.0032	0.80
MPI-ESM_0043	-0.0004	0.98	-0.0084	0.43	-0.017	0.11
MPI-ESM_0050	-0.0002	0.99	0.00021	0.99	-0.012	0.32
EC-Earth3-veg-LR	<b>-0.13</b>	$4 \times 10^{-7}$	-0.025	0.15	<b>-0.036</b>	0.047
HadCM3-M2.1d	0.012	0.47	-0.0044	0.56	-0.020	0.098
KCM	<b>0.033</b>	$6 \times 10^{-5}$	-0.0018	0.73	-0.0045	0.22
CCSM3	<b>0.054</b>	0.0017	<b>-0.02</b> <sup>‡</sup>	0.03	-0.010	0.11
CESM1.2.1	<b>0.013</b>	0.00028	0.0010	0.61	0	0

<sup>†</sup>The trend for the mean AMOC time series is statistically significant over the whole run length, yet there is no statistically significant trend for the final 4,000 yrs (4-0 ka BP). <sup>‡</sup>If the analysis period is extended back to 7ka, the CCSM3  $\sigma$  trend is not statistically significant.

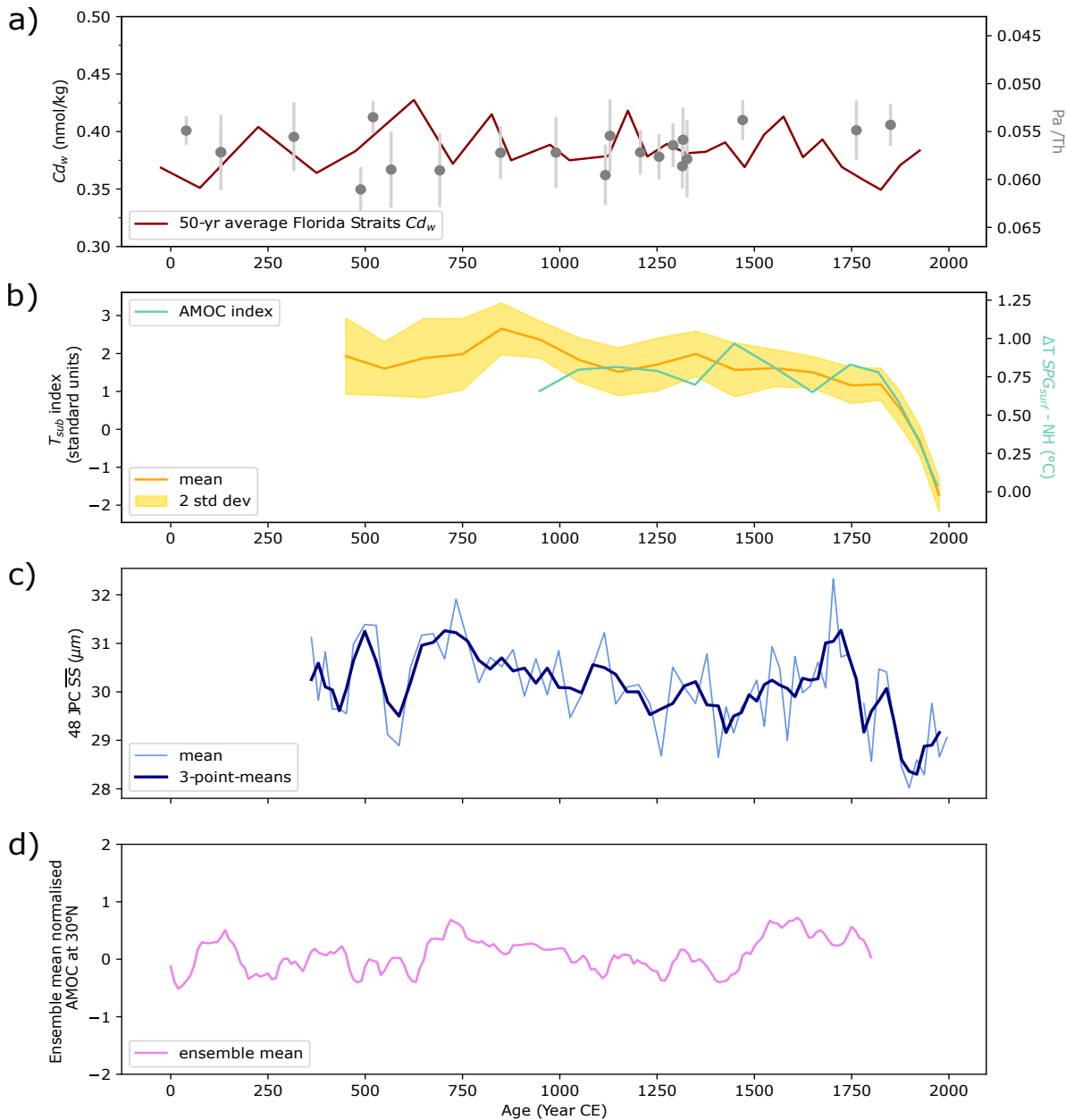


**Figure S1.** Indicators of the AMOC variability for the past 2,000 years. (a) 50-year average Florida Straits seawater cadmium data (dark red line) taken from Valley et al. (2022) shown on the left y-axis;  $Pa/Th$  data (grey dots) taken from Lippold et al. (2019) shown on the right y-axis; (b) Subsurface temperature AMOC index (orange line) taken from Thornalley et al. (2018) shown on the left y-axis; the AMOC index, namely the difference between subpolar gyre and Northern Hemisphere temperature anomalies (light green line) taken from Rahmstorf et al. (2015) shown on the right y-axis; (c) Mean grain size sortable silt (SS) taken from Thornalley et al. (2018); (d) normalised (z-score) ensemble mean AMOC taken from Fig 4(a).

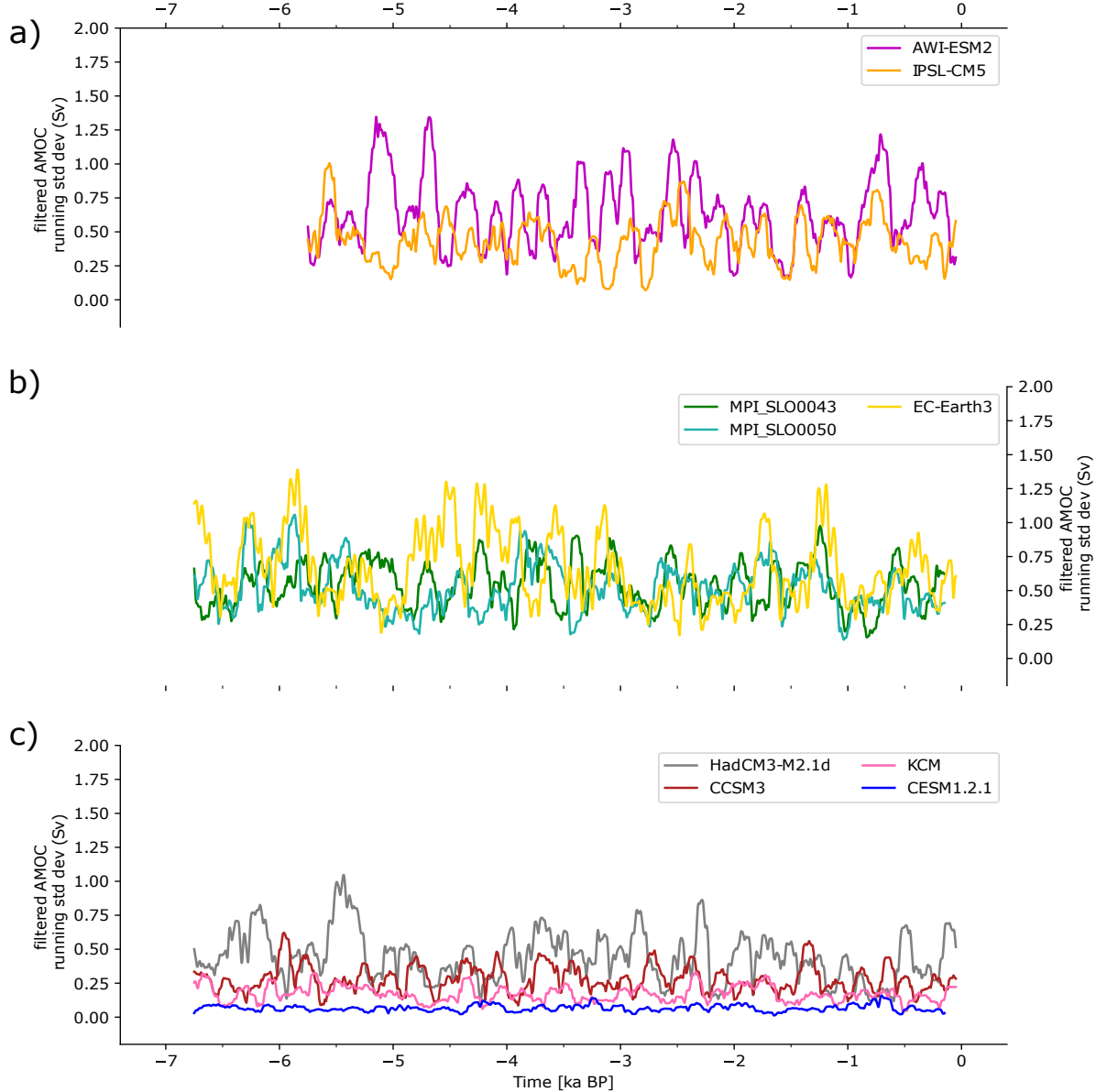


**Figure S2.** As Fig. 3, but showing the 100-yr running standard deviation of the band-pass (25–75 yr) filtered overall maximum AMOC strength at 30°N below 500 m. This focuses solely on multidecadal variability, so all values are lower than in Fig. 3. The trend for each simulation is listed in Table S1.